Received: 23 March 2024 | Revised: 17 July 2024 | Accepted: 13 August 2024
DOI: 10.4218/etrij.2024-0137

SPECIAL ISSUE

ETRI Journal WILEY

Fabrication of low-loss symmetrical rib waveguides based on *x*-cut lithium niobate on insulator for integrated quantum photonics

Hong-Seok Kim[1] | **Guhwan Kim**[1,2] | **Tetiana Slusar**[1] | **Jinwoo Kim**[1] | **Jiho Park**[1] | **Jaegyu Park**[1] | **Hyeon Hwang**[3] | **Woojin Noh**[3] | **Hansuek Lee**[3] | **Min-Kyo Seo**[3] | **Kiwon Moon**[1] | **Jung Jin Ju**[1]

[1]Quantum Technology Research Division, Electronics and Telecommunications Research Institute, Daejeon, Republic of Korea

[2]Department of Electrical and Computer Engineering, Sungkyunkwan University, Suwon, Republic of Korea

[3]Department of Physics, Korea Advanced Institute of Science and Technology, Daejeon, Republic of Korea

Correspondence
Hong-Seok Kim, Quantum Technology Research Division, Electronics and Telecommunications Research Institute Daejeon, Republic of Korea.
Email: hongseok@etri.re.kr

Abstract
Lithium niobate on insulator (LNOI) is a promising material platform for applications in integrated quantum photonics. A low optical loss is crucial for preserving fragile quantum states. Therefore, in this study, we have fabricated LNOI rib waveguides with a low optical propagation loss of 0.16 dB/cm by optimizing the etching conditions for various parameters. The symmetry and smoothness of the waveguides on *x*-cut LNOI are improved by employing a shallow etching process. The proposed method is expected to facilitate the development of on-chip quantum photonic devices based on LNOI.

KEYWORDS
integrated quantum photonics, lithium niobate on insulator, low-loss rib waveguide, microring resonator, shallow etching

1 | INTRODUCTION

Lithium niobate on insulator (LNOI) is an attractive platform for advancing both classical and quantum photonic integrated circuits, owing to its exceptional optical properties. The high index contrast and small cross-section of submicron-thick LNOI enable tight mode confinement, which is a critical factor in fabricating compact integrated photonic devices [1, 2]. Tight mode confinement enhances the efficiency of nonlinear frequency conversion processes, such as second-harmonic generation (SHG), sum-frequency generation (SFG), and difference-frequency generation [3, 4]. Moreover, it maximizes the generation of entangled photon pairs in the spontaneous parametric down-conversion (SPDC) process, which is essential for quantum communications, quantum sensing, and quantum computing applications [5–7]. The efficiency of these processes can be improved by fabricating periodically poled lithium niobate (PPLN) waveguides to establish quasi-phase-matching conditions for the interacting waves [3, 6, 8]. Thus, a waveguide based on LNOI is a remarkable platform for compact integrated quantum photonic devices [2].

Multiple PPLN waveguide devices have been demonstrated based on the *x*-cut LNOI, which is preferable to the *z*-cut LNOI due to the electrode placement and mode losses. In contrast to the *x*-cut LNOI, which uses planar electrodes on the surface, the *z*-cut LNOI typically requires the fabrication of buried ground electrodes for poling and high-speed electro-optic modulators. This is challenging and can cause additional optical mode losses [9, 10].

To ensure the highly efficient performance of the waveguide, strict requirements are imposed, particularly to the surface quality. The surface quality criteria typically focus on achieving low sidewall roughness, which is crucial for minimizing scattering-induced propagation losses and ensuring high-efficiency optical transmission, frequency conversion, and entanglement photon generation in quantum photonics devices [2]. Although the etching of lithium niobate (LN) thin films to fabricate waveguide structures has been extensively studied, and various techniques have been applied, achieving smooth surfaces remains challenging [11, 12].

The propagation axis of the *x*-cut PPLN waveguide must be aligned along the *y*-axis and perpendicular to the inverted ferroelectric domains along the *z*-axis [3, 13, 14]. However, the LN crystal structure is strongly anisotropic in the *z*-direction, which causes asymmetric etching characteristics along the $+z$- and $-z$-directions [15]. Therefore, the roughness and angle of the *z*-sidewalls can vary depending on the sign of *z*. In such waveguides, careful control and optimization of the sidewall roughness are essential because quantum entanglement is easily affected by loss-induced decoherence [2]. Nevertheless, a comprehensive study addressing the issue of asymmetric sidewall roughness is yet to be conducted.

Herein, we report a fabrication method for improving the sidewall smoothness and symmetry of the *x*-cut LNOI rib waveguide. We obtained a high intrinsic quality factor (*Q* factor) of 2.58×10^6 corresponding to the low optical propagation loss of 0.16 dB/cm in our LNOI microring resonator. Various fabrication steps, including rib waveguide dry etching, wet cleaning, and shallow etching, were optimized. A shallow etching process with an Ar/O_2 gas mixture was applied as a novel method to improve the asymmetric lateral etching quality and roughness of *y*-guided waveguides on the *x*-cut LNOI. This method is currently applied in the fabrication of our SHG, SFG, and SPDC devices on the *x*-cut LNOI [16]. We expect that this study will contribute to the development of on-chip quantum photonic devices using LNOI.

2 | EXPERIMENTAL RESULTS

2.1 | Waveguide fabrication process

We use a 600-nm-thick *x*-cut LN on top of a 4.7-μm-thick silicon dioxide (SiO_2) and intrinsic ($\rho > 10000\ \Omega$ cm) silicon handle wafers from NanoLN as shown in Figure 1A. A hydrogen silsesquioxane (HSQ)-based resist (FOx-16) is

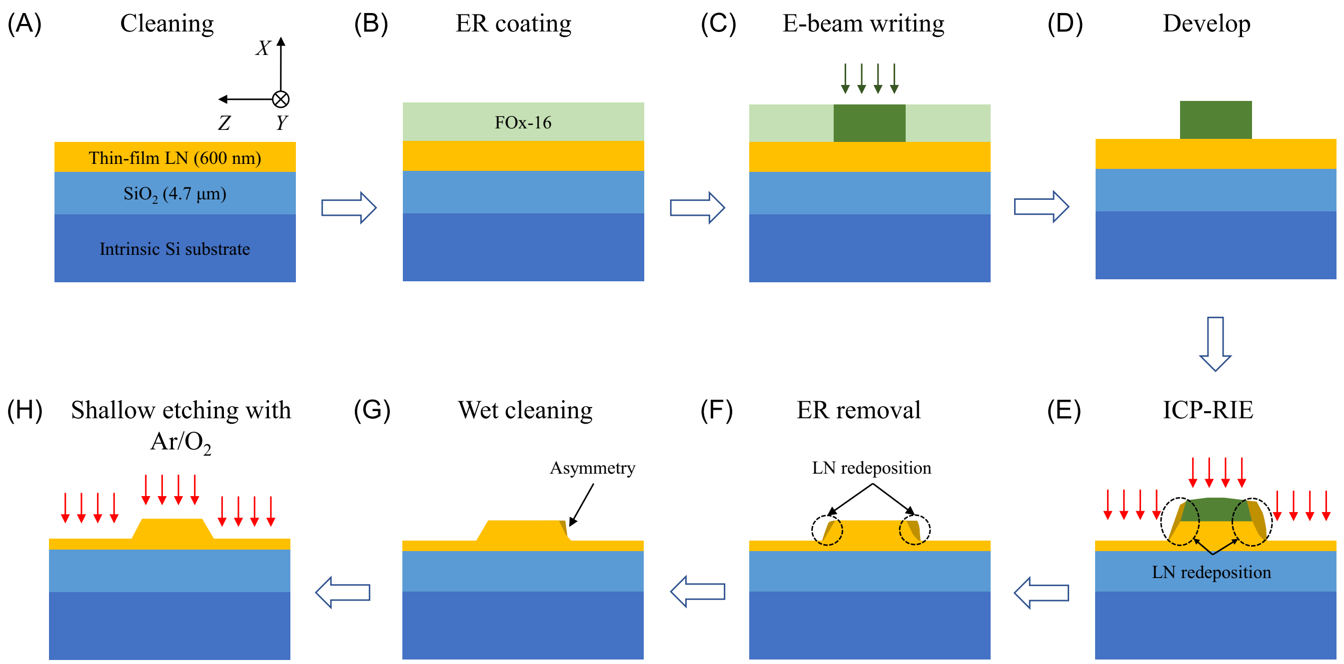

FIGURE 1 Schematic of the fabrication process of an lithium niobate on insulator (LNOI) rib waveguide. (A) Preparation of an LNOI wafer; (B) FOx-16 spin-coating; (C) e-beam lithography; (D) develop; (E) inductively coupled plasma (ICP)-reactive ion etching (RIE) process; (F) ER removal; (G) wet cleaning. An asymmetrical cross-section of the waveguide can be observed after etching due to lithium niobate (LN) crystal anisotropy. See main text for details. (H) Shallow etching process with Ar/O_2 gases.

spin-coated onto an LNOI substrate pretreated with oxygen plasma and hexamethyldisilazane to enhance adhesion (Figure 1B), followed by the application of an anti-charging agent to prevent charge accumulation. The rib waveguide pattern is defined in the FOx-16 resist using standard electron beam lithography with a beam acceleration voltage of 100 keV (EBPG 5000 plus), which mitigates proximity effects and increases the exposure precision (Figure 1C). After development, the LN thin film is dry-etched with argon plasma (Ar^+) using a commercial inductively coupled plasma (ICP) reactive ion etching (RIE) system (Figures 1D,E). Following the plasma etching, the remaining HSQ on the rib is removed by buffered oxide etchant (Figure 1F). Wet cleaning in a mixture of hydrogen peroxide and ammonium hydroxide is performed to remove by-products redeposited during the etching process (Figure 1G). Subsequently, shallow etching with Ar and O_2 gases is implemented using ICP-RIE, aiming to improve the sidewall symmetry and smoothness of the rib waveguide (Figure 1H).

2.1.1 | ICP-RIE process

Dry etching is suitable for fabrication of high-quality LNOI waveguides owing to its high anisotropy and controllability. Among the dry etching techniques, focused ion beam (FIB) milling [17, 18], fluorine-based RIE [19, 20], and argon-based ICP-RIE (argon ion milling) [8, 21–23] have been used to etch LNOI [1, 24]. FIB enables the directional etching of LN thin films with high precision; however, scaling up the process to accommodate large wafer sizes is challenging [1]. This issue can be addressed using RIE-based techniques. However, RIE, which employs argon and fluorine-based mixtures, can cause LN surface contamination by lithium fluoride (LiF) redeposition. The LiF redeposition is difficult to eliminate; thus, it increases LN sidewall roughness and scattering losses [1, 24]. By contrast, argon-based ICP-RIE is a purely physical sputtering method that results in a less severe redeposition of chemical by-products. A high *Q* factor value of 10 million in LNOI was achieved using argon-based ICP-RIE [22]. Therefore, argon-plasma-based ICP-RIE is preferred for etching LNOI for integrated photonics [21–23, 25, 26]. Despite that, ICP-RIE is a complex process that requires the careful optimization of process parameters, such as ICP and RIE powers, working pressure, etching duration, design geometry, and temperature, to achieve a low-loss waveguide [11, 12].

The sidewall roughness of a waveguide can be improved by increasing the ICP power, which enhances the plasma density. The RIE generator controls the argon-ion bombardment (kinetic) energy, which should be higher than the binding energy of the LN crystal. Similarly, a higher RIE power can reduce the sidewall roughness [11]. Moreover, if the RIE bias voltage is sufficiently high, the redeposition rate decreases because of the increased reetch rate of the by-products accumulated on the sidewall. At the same time, high-energy ions can be reflected from the sidewalls and etch the slab adjacent to the rib, forming deep trenches [12]. When the ICP and RIE powers are excessively high, the etching reproducibility and rate become unstable. Thus, the power increase is limited. We succeeded in determining the stable conditions at an ICP/RIE power of 150 W/250 W (an etch rate of ~40 nm/min and a mask selectivity of 1:1), providing reproducible fabrication of low redeposition and low roughness waveguides. The remaining redeposition can be effectively removed and smoothed through the following wet cleaning and shallow etching processes, as discussed later. To enhance mask selectivity, we cooled the substrate temperature to 5 °C [11].

Regarding the working pressure, the collision rate of argon ions decreases at lower pressures, resulting in a longer mean free path and higher kinetic energy, which improves the etching efficiency. By contrast, a higher working pressure can increase the redeposition rate due to the higher rate of atom recollisions [11]. We conducted a series of etching processes at working pressures ranging from 1 to 5 mTorr. At higher pressures of 5 and 4 mTorr, the redeposition rate was too high for the redeposited material to be completely removed from the sidewalls using the standard wet cleaning process. In contrast, at lower pressures of 3 and 2 mTorr, the redeposited material was efficiently removed via posttreatment. However, consistent results were obtained only at 2 mTorr. Meanwhile, 1 mTorr pressure was insufficient for our ICP-RIE system to maintain a stable plasma. Therefore, a working pressure of 2 mTorr was employed, whereas the base pressure was approximately $7–8 \times 10^{-7}$ Torr.

2.1.2 | Wet cleaning process

In the ICP-RIE process, the redeposition of LN material can significantly affect the sidewall roughness. When argon ions with kinetic energy exceeding the binding energy of the LN constituents collide with the LN surface, the constituents are ejected and scattered in all directions. Some of these scattered constituents (by-products) can adhere back to the surface of the rib, forming redeposition, which increases the sidewall roughness [11, 12]. The high roughness of the rib sidewalls strongly scatters the guided light, thereby deteriorating the optical performance of the waveguide. These redeposition-

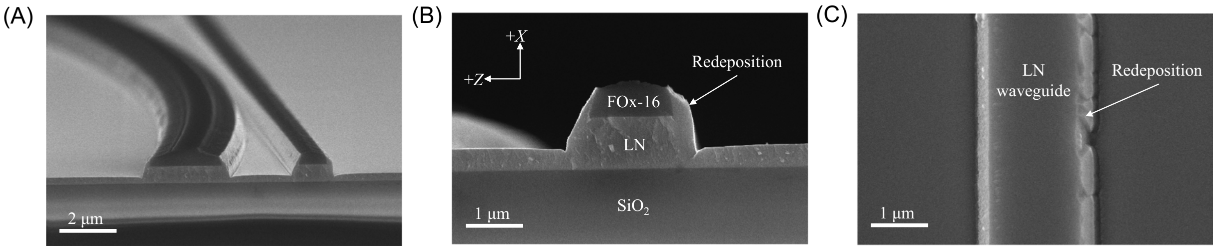

FIGURE 2 (A) Scanning electron microscopy (SEM) image of the lithium niobate on insulator (LNOI) rib waveguides after etching. (B) Enlarged cross-sectional view of the straight waveguide in (A). (C) Top-view SEM image of the waveguide after FOx-16 removal. The redeposition on the sidewall was observed.

induced by-products were observed in scanning electron microscopy (SEM) images taken before (Figure 2A,B) and after (Figure 2C) removal of the FOx-16 layer.

We use a solvent consisting of ammonium hydroxide (NH_4OH) and hydrogen peroxide (H2O2) in a ratio of 1:1 to remove the LN redeposition induced by the ICP-RIE process. This solvent mixture has also been employed for the wet etching of LN [15]. Therefore, a wet cleaning process based on this solvent mixture is an effective way to remove the LN redeposition [11, 25]. Wet cleaning is performed by using the solvent mixture at 85 °C for 1 h. Figure 3A,B shows the bright- and dark-field optical microscopy (OM) images of the rib waveguide before wet cleaning, respectively. By-products on the rib sidewall due to the LN redeposition were observed in both OM images. After applying the wet treatment, the sidewalls roughness was reduced due to the removal of by-products (Figure 3C,D).

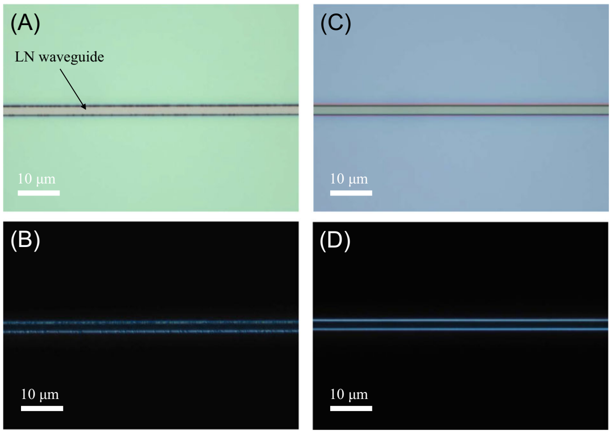

FIGURE 3 Bright- and dark-field optical microscopy (OM) images of the lithium niobate on insulator (LNOI) rib waveguide before (A,B) and after (C,D) wet cleaning.

2.1.3 | Asymmetrically etched waveguide

We fabricated two perpendicular rib waveguides spanning the *y*- and *z*-axes of the LN thin film, as shown in the top-view SEM image in Figure 4A. Notable asymmetric etching can be observed on the sidewalls of the *y*-oriented waveguide (vertical), with higher roughness on the –*z*-sidewall (denoted by yellow arrows) compared with the +*z*-sidewall. This could be due to the strong anisotropic properties of LN along the *z*-axis [15]. Magnified side views of the −*z*-sidewall of the *y*-oriented rib waveguide and cross-sectional image of the same rib are shown in Figure 4B,C, respectively. The asymmetry of the rib and its roughness, which have a detrimental effect on the light propagation efficiency, were observed. Residual by-products remained on the −*z*-sidewall even after wet cleaning. Since the anisotropy of the LN along the *y*-axis is less pronounced, both the −*y*- and +*y*-sidewalls of the *z*-oriented waveguide (horizontal) exhibit similar roughness, with only slight differences observed in their

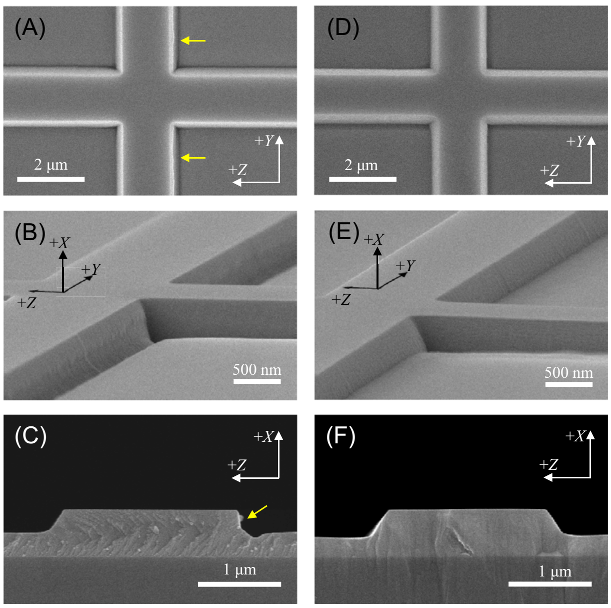

FIGURE 4 Scanning electron microscopy (SEM) images of (A) top, (B) tilted, and (C) cross-sectional views of cross-shape LN rib structure. (D–F) SEM images of the same waveguide after the shallow etching process corresponding to (A), (B), and (C), respectively.

angles. As our primary focus is on the y-oriented waveguide, which can satisfy quasi-phase-matching conditions after periodic poling along the z-axis, we will further consider only this geometry [13].

2.1.4 | Shallow etching process

A shallow etching process was further performed on the same waveguide using ICP-RIE to mitigate the asymmetric etching effect. The etching was done with an ICP/RIE power of 300 W/400 W at a gas flow rate of Ar/O2 = 5 sccm/15 sccm. The etch rates for the depth and top width of the rib were 6.7 and 50 nm/min, respectively. The depth of the shallow-etched layer was 20 nm. Figure 4D,E,F shows the corresponding SEM images of the top, $-z$-sidewall, and cross-section of the rib, respectively, obtained after the shallow etching. As shown, the redepositions on the $-z$ side were completely removed by the shallow etching, improving the waveguide symmetry.

As niobium (Nb) atoms are heavy and difficult to be carried away from the LN surface during etching, they are considered to be the main constituents of the redeposited material. By introducing O2 gas during the shallow etching process, it bonds with Nb atoms and results in their effective elimination from the sidewall. Therefore, by applying the shallow etching with a low Ar/O2 gas ratio, the symmetric and smooth rib waveguides can be fabricated. Furthermore, this approach can improve the asymmetry of the y-oriented rib, as shown in Figure 4D. The overall parameters of the optimized fabrication process are listed in Table 1.

2.2 | Optical characterization

Figure 5A shows a cross-sectional schematic view of the LNOI microring resonator. After the shallow etching, the total thickness of LNOI (h_2) and the height of the rib (h_1) were 580 nm and 330 nm, respectively. The angle of the sidewall was defined as 55°. We fabricated a waveguide-coupled microring with a radius of 200 μm, a coupling gap of ~500 nm (between the top surfaces), and a top width (w_t) of 2.1 μm to measure the Q factor that directly reflects the waveguide propagation losses (Figure 5B). Figure 5C,D displays the SEM images of the right and left sidewalls of the microring, respectively, which indicate the smooth surface morphology on both z sides.

A schematic diagram of the optical setup is shown in Figure 6A. The optical transmission spectrum of the resonator was measured in the wavelength range of 1540 nm–1560 nm by scanning with a tunable external-cavity diode laser (ECDL, TLB-6728). Simultaneously, we measured the transmission of a Mach–Zehnder interferometer (MZI) with a narrow bandwidth of 204 MHz to obtain a precise resonant mode linewidth [25, 27]. The rib waveguide facet was butt-coupled using a lensed fiber (OZ Optics). The transmitted signals were detected by an avalanche photodiode (APD).

The measured optical transmission spectrum of the microring resonator and MZI are shown in the top and bottom panels of Figure 6B, respectively. The loaded Q factor was obtained as $Q_l = 1.31 \times 10^6$ near the wavelength of

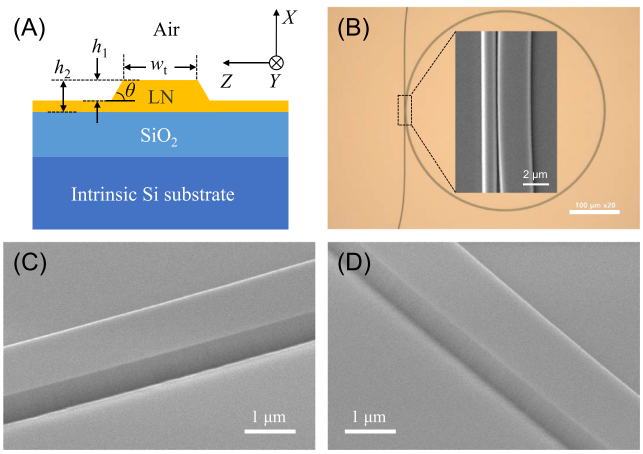

FIGURE 5 (A) Cross-sectional schematic of the lithium niobate on insulator (LNOI) microring resonator. (B) Optical microscopy (OM) image of the microring. Inset: Scanning electron microscopy (SEM) image of coupling point with bus waveguide. (C,D) SEM images of both sides of the resonator.

TABLE 1 Fabrication process parameters.

Process	ICP power (W)	RIE power (W)	Pressure (mTorr)	Gas flow rate (sccm)	Temperature (°C)
ICP-RIE	150	250	2	15 (Ar)	5
Process	**Solvent**	**Time (min)**	**Temperature (°C)**		
Wet cleaning	NH_4OH: H_2O_2 = 1:1	60	85		
Process	**ICP power (W)**	**RIE power (W)**	**Pressure (mTorr)**	**Gas flow rate (sccm)**	**Temperature (°C)**
Shallow etching	300	400	7	5/15 (Ar/O_2)	18

Abbreviations: ICP, inductively coupled plasma; RIE, reactive ion etching.

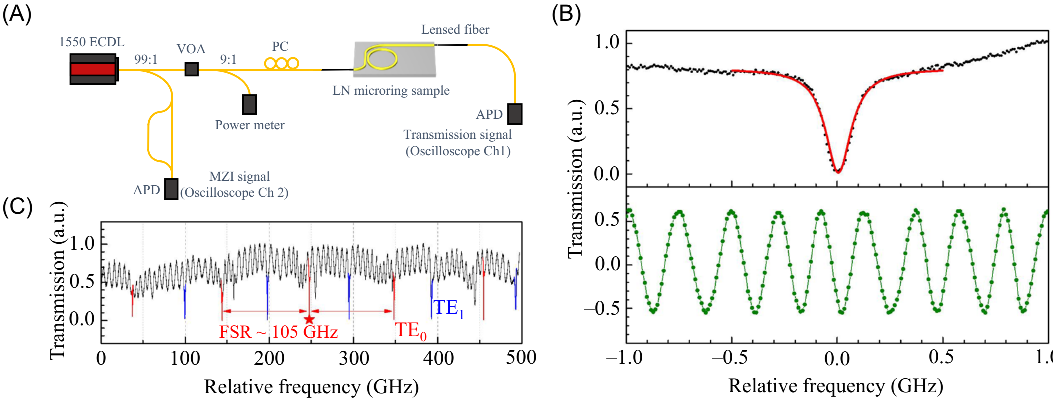

FIGURE 6 (A) Schematic of the optical measurement setup. APD, avalanche photodiode; ECDL, external-cavity diode laser; MZI, Mach–Zehnder interferometer; PC, polarization controller; VOA, variable optical attenuator. (B) Top: normalized transmission spectrum of the microring resonator corrected for background slope. The black dots and the red solid line represent the experimental data points and the Lorentzian fitting curve, respectively. Bottom: MZI transmission signal. (C) Wide range transmission spectrum of the microring resonator. The peak denoted by the red star symbol is depicted in (B).

1550 nm by fitting with a Lorentzian function. The intrinsic Q factor (Q_i) is related to the measured Q_l, as follows:

$$Q_i = \frac{2Q_l}{1 \pm \sqrt{T_0}}, \tag{1}$$

where T_0 is the normalized on-resonance transmission, and $+$ and $-$ indicate the under- and over-coupled regimes, respectively. In the critical coupling regime, T_0 can be approximated as zero, resulting in $Q_i \approx 2Q_l$. In Figure 6B, T_0 reaches approximately zero, indicating that the microring resonator is in the critical coupling regime. Thus, the intrinsic Q factor was obtained as $Q_i = 2.58 \times 10^6$.

The mode index can be expressed by the following relationship [21, 28]:

$$n_g = \frac{c}{\mathrm{FSR}_f \cdot 2\pi R}, \tag{2}$$

where R is the radius of the microring, c is the speed of light, and λ is the resonant wavelength. The free-spectral range in the frequency span ($\mathrm{FSR}_f = c/\lambda^2 \cdot \mathrm{FSR}_\lambda$, where FSR_λ is the free-spectral range in the wavelength span) was defined as 105 GHz for the red-colored peaks in Figure 6C. Based on this relationship, we obtained a value of $n_g = 2.3$. The mode index for the fundamental TE mode (TE_0) of the microring resonator was calculated to be 2.31, which agrees well with the experimental data. The FSR_f of the blue peaks was ~99 GHz, which corresponds to the TE_1 mode with $Q_l = 5.52 \times 10^5$. The optical propagation loss can be obtained using the following relationship:

$$L_p = 10 \cdot \frac{2\pi n_g}{Q_i \lambda} \cdot \log e. \tag{3}$$

Consequently, the propagation loss of our rib waveguide for the TE_0 mode was estimated to be 0.16 dB/cm, which is comparable to the previously reported values on the LNOI in the telecom band [29–32]. If we apply the annealing process at temperatures above 500 °C, the propagation optical loss can be further reduced because of the improved crystallinity of the LNOI [32, 33]. However, this approach is challenging for the PPLN waveguide devices because the periodic poled-domain structure can easily degrade or backswitch at high temperatures [34].

3 | CONCLUSION

We described a fabrication method for a low-loss symmetric rib waveguide based on the *x*-cut LNOI, which is a facile approach for the on-chip integration of high-performance passive and active devices with planar electrodes. A wet-etching process using a mixture of ammonium hydroxide and hydrogen peroxide effectively removed the redeposition-induced by-products on the sidewalls of the rib waveguide. However, in the case of the rib waveguide spanning along the *y*-axis, an asymmetric etching effect on the $-z$-sidewall was observed owing to the LN crystal anisotropy. The sidewall roughness of the *y*-oriented waveguide is an important factor in the fabrication of SHG, SFG, and SPDC devices using *x*-cut PPLN waveguides for quantum applications. We showed that applying the newly suggested shallow etching with Ar/O_2 can improve the rib waveguide sidewall symmetry and smoothness. Consequently, a high intrinsic Q factor of 2.58×10^6 was achieved, which corresponds to a low propagation loss of 0.16 dB/cm. We expect that our results will contribute to the development of highly efficient on-chip quantum devices based on LNOI.

ACKNOWLEDGMENTS

This study was supported by the Institute of Information & Communications Technology Planning & Evaluation (IITP) grant funded by the Korean government (MSIT) (Grant 2022-0-00463, Development of a quantum repeater in optical fiber networks for quantum internet), (Grant 2021-0-00552, Development of PPLN waveguide devices for single-photon wavelength conversions), and by the Electronics and Telecommunications Research Institute (ETRI) grant funded by the Korean government (Grant 24ZS1220, Proprietary basic research on computing technology for the disruptive innovation of computational performance). We are grateful to Dr. Min-Su Kim and Dr. Jae-Pil So for their valuable discussions and comments.

CONFLICT OF INTEREST STATEMENT

The authors declare that there are no conflicts of interest.

ORCID

Hong-Seok Kim https://orcid.org/0000-0002-2356-8403
Tetiana Slusar https://orcid.org/0000-0001-8837-6165

REFERENCES

1. D. Zhu, L. Shao, M. Yu, R. Cheng, B. Desiatov, Y. H. Xin, Y. Hu, J. Holzgrafe, S. Ghosh, A. Shams-Ansari, E. Puma, N. Sinclair, C. Reimer, M. Zhang, and M. Lončar, *Integrated photonics on thin-film lithium niobate*, Adv. Opt. Photon. **13** (2021), no. 2, 242–352.
2. S. Saravi, T. Pertsch, and F. Setzpfandt, *Lithium niobate on insulator: an emerging platform for integrated quantum photonics*, Adv Opt Mater **9** (2021), no. 22, 2100789.
3. C. Wang, C. Langrock, A. Marandi, M. Jankowski, M. Zhang, B. Desiatov, M. M. Fejer, and M. Lončar, *Ultrahigh-efficiency wavelength conversion in nanophotonic periodically poled lithium niobate waveguides*, Optica **5** (2018), no. 11, 1438–1441.
4. M. Younesi, R. Geiss, S. Rajaee, F. Setzpfandt, Y.-H. Chen, and T. Pertsch, *Periodic poling with a micrometer-range period in thin-film lithium niobate on insulator*, JOSA B **38** (2021), no. 3, 685–691.
5. S. Tanzilli, W. Tittel, H. De Riedmatten, H. Zbinden, M. Paolo Baldi, M. DeMicheli, D. B. Ostrowsky, and N. Gisin, *Ppln waveguide for quantum communication*, Eur Phys. J. D-Atomic. Molecular Opt. Plasma Phys. **18** (2002), 155–160.
6. Y. Qi and Y. Li, *Integrated lithium niobate photonics*, Nanophoton. **9** (2020), no. 6, 1287–1320.
7. J. Kim, J. Park, H.-S. Kim, G. Kim, T. V. Slusar, J. Kim, J. Park, K. Moon, and J. J. Ju, In *The role of state preparation in time-bin entangled photon pair generation for quantum communication, quantum computing, communication, and simulation IV*, P. R. Hemmer, A. L. Migdall (eds.) Vol. **12911**, SPIE, 2024, 401–405.
8. X. Wang, X. Jiao, B. Wang, Y. Liu, X.-P. Xie, M.-Y. Zheng, Q. Zhang, and J.-W. Pan, *Quantum frequency conversion and single-photon detection with lithium niobate nanophotonic chips*, npj Quantum Inform. **9** (2023), no. 1, 38.
9. M. Zhang, C. Wang, P. Kharel, D. Zhu, and M. Lončar, *Integrated lithium niobate electro-optic modulators: when performance meets scalability*, Optica **8** (2021), no. 5, 652–667.
10. J. Zhao, M. Rüsing, M. Roeper, L. M. Eng, and S. Mookherjea, *Poling thin-film x-cut lithium niobate for quasi-phase matching with sub-micrometer periodicity*, J. Appl. Phys. **127** (2020), no. 19, 193104.
11. G. Ulliac, V. Calero, A. Ndao, F. I. Baida, and M.-P. Bernal, *Argon plasma inductively coupled plasma reactive ion etching study for smooth sidewall thin film lithium niobate waveguide application*, Opt. Mater. **53** (2016), 1–5.
12. F. Kaufmann, G. Finco, A. Maeder, and R. Grange, *Redeposition-free inductively-coupled plasma etching of lithium niobate for integrated photonics*, Nanophoton. **12** (2023), no. 8, 1601–1611.
13. J. Zhao, C. Ma, M. Rüsing, and S. Mookherjea, *High quality entangled photon pair generation in periodically poled thin-film lithium niobate waveguides*, Phys. Rev. Lett. **124** (2020), no. 16, 163603.
14. Y. Niu, C. Lin, X. Liu, Y. Chen, X. Hu, Y. Zhang, X. Cai, Y.-X. Gong, Z. Xie, and S. Zhu, *Optimizing the efficiency of a periodically poled lnoi waveguide using in situ monitoring of the ferroelectric domains*, Appl. Phys. Lett. **116** (2020), no. 10, 101104.
15. R. Zhuang, J. He, Y. Qi, and L. Yang, *High-q thin-film lithium niobate microrings fabricated with wet etching*, Adv. Mater. **35** (2023), no. 3, 2208113.
16. G. Kim, T. V. Slusar, H.-S. Kim, J. Kim, J. Park, J. T. Kim, J. Park, K. Moon, M.-H. Lee, and J. J. Ju, In *Generating entangled photon pairs in thin film lithium niobate for quantum communication, integrated optics: devices, materials, and technologies XXVIII*, S. M. García-Blanco, P. Cheben (eds.) Vol. **PC12889**, SPIE, 2024.
17. F. Lacour, N. Courjal, M.-P. Bernal, A. Sabac, C. Bainier, and M. Spajer, *Nanostructuring lithium niobate substrates by focused ion beam milling*, Opt. Mater. **27** (2005), no. 8, 1421–1425.
18. G. Si, A. J. Danner, S. L. Teo, E. J. Teo, J. Teng, and A. A. Bettiol, *Photonic crystal structures with ultrahigh aspect ratio in lithium niobate fabricated by focused ion beam milling*, J. Vac. Sci. Technol. B **29** (2011), no. 2.
19. H. Hu, A. P. Milenin, R. B. Wehrspohn, H. Hermann, and W. Sohler, *Plasma etching of proton-exchanged lithium niobate*, J. Vacuum Sci. Technol. A **24** (2006), no. 4, 1012–1015.
20. W. J. Park, W. S. Yang, W. K. Kim, H. Y. Lee, J.-W. Lim, M. Isshiki, and D. H. Yoon, *Ridge structure etching of linbo3 crystal for optical waveguide applications*, Opt. Mater. **28** (2006), no. 3, 216–220.
21. A. Pan, H. Changran, C. Zeng, and J. Xia, *Fundamental mode hybridization in a thin film lithium niobate ridge waveguide*, Opt. Express **27** (2019), no. 24, 35659–35669.
22. M. Zhang, C. Wang, R. Cheng, A. Shams-Ansari, and M. Lončar, *Monolithic ultra-high-q lithium niobate microring resonator*, Optica **4** (2017), no. 12, 1536–1537.

23. Q. Luo, R. Chen Yang, Z. H. Zhang, D. Zheng, H. Liu, Y. Xuanyi, F. Gao, F. Bo, Y. Kong, et al., *On-chip erbium-doped lithium niobate microring lasers*, Opt. Lett. **46** (2021), no. 13, 3275–3278.
24. Z. Wang, C. Wang, and H. Yu, *Advances in nonlinear photonic devices based on lithium niobate waveguides*, J. Phys. D Appl. Phys. **56** (2023), no. 8, 083001.
25. H. Hwang, H. Heo, K. Ko, M. R. Nurrahman, K. Moon, J. J. Ju, S.-W. Han, H. Jung, H. Lee, and M.-K. Seo, *Electro-optic control of the external coupling strength of a high-quality-factor lithium niobate micro-resonator*, Opt. Lett. **47** (2022), no. 23, 6149–6152.
26. H. Hwang, M. R. Nurrahman, H. Heo, K. Ko, K. Moon, J. J. Ju, S.-W. Han, H. Jung, H. Lee, and M.-K. Seo, *Hyperband electro-optic modulator based on a two-pulley coupled lithium niobate racetrack resonator*, Opt. Lett. **49** (2024), no. 3, 658–661.
27. J. Li, H. Lee, K. Y. Yang, and K. J. Vahala, *Sideband spectroscopy and dispersion measurement in microcavities*, Opt. Express **20** (2012), no. 24, 26337–26344.
28. W. Bogaerts, P. De Heyn, T. Van Vaerenbergh, and K. De Vos, *Shankar Kumar Selvaraja, tom Claes, Pieter Dumon, Peter Bienstman, dries Van Thourhout, and Roel Baets, silicon microring resonators*, Laser Photon. Rev. **6** (2012), no. 1, 47–73.
29. S. Y. Siew, E. J. H. Cheung, H. Liang, A. Bettiol, N. Toyoda, B. Alshehri, E. Dogheche, and A. J. Danner, *Ultra-low loss ridge waveguides on lithium niobate via argon ion milling and gas clustered ion beam smoothening*, Opt. Express **26** (2018), no. 4, 4421–4430.
30. I. Krasnokutska, J.-L. J. Tambasco, X. Li, and A. Peruzzo, *Ultra-low loss photonic circuits in lithium niobate on insulator*, Opt. Express **26** (2018), no. 2, 897–904.
31. R. Luo, Y. He, H. Liang, M. Li, and Q. Lin, *Highly tunable efficient second-harmonic generation in a lithium niobate nanophotonic waveguide*, Optica **5** (2018), no. 8, 1006–1011.
32. J. Shi, Z. Ye, M. Lv, D. Ge, L. Zhang, S. Zhu, and G. Cui, *Reduced material loss caused by electron beam lithography in thin-film lithium niobate through post-process annealing*, Opt. Mater. **149** (2024), 115049.
33. A. Shams-Ansari, G. Huang, L. He, Z. Li, J. Holzgrafe, M. Jankowski, M. Churaev, P. Kharel, R. Cheng, D. Zhu, N. Sinclair, B. Desiatov, M. Zhang, T. J. Kippenberg, and M. Lončar, *Reduced material loss in thin-film lithium niobate waveguides*, APL Photon. **7** (2022), no. 8, 081301.
34. Y. Jiao, Z. Shao, S. Li, X. Wang, F. Bo, J. Xu, and G. Zhang, *Improvement on thermal stability of nano-domains in lithium niobate thin films*, Crystals **10** (2020), no. 2, 74.

AUTHOR BIOGRAPHIES

Hong-Seok Kim received his BS and PhD degrees (integrated MS and PhD program) in physics from Korea University, Republic of Korea, in 2009 and 2016, respectively. From 2016 to 2020, he was a postdoctoral research fellow at the Topological Quantum Devices Center of Gwangju Institute of Science and Technology, Republic of Korea. Since 2021, he has been a senior researcher at the Electronics and Telecommunications Research Institute, Republic of Korea. His research interests include mesoscopic quantum physics and integrated photonic devices for quantum information applications.

Guhwan Kim received his BS degree in nano-optics engineering from Korea Polytechnic University, Siheung, Republic of Korea, in 2019. Currently, he is a PhD candidate in electrical and computer engineering from Sungkyunkwan University, Suwon, Republic of Korea. In 2022, he joined the Electronics and Telecommunications Research Institute, Daejeon, Republic of Korea, as a graduate research assistant. His research interests include photonic integrated circuits, nonlinear optics, and optoelectronic devices.

Tetiana Slusar received her BS and MS degrees in applied physics from the National Aviation University (NAU) in Kyiv, Ukraine, in 2009 and 2011, respectively. She began her PhD in 2011 at the NAU and the Lashkaryov Institute of Semiconductor Physics, National Academy of Science, Kyiv, Ukraine. Since 2013, she has been working at the Electronics and Telecommunications Research Institute, Daejeon, Republic of Korea, where she is now a senior researcher. Her research interests include materials science, nonlinear optics, and quantum optics.

Jinwoo Kim received his master of physics degree from the University of Oxford, Oxford, UK, in 2022. He has worked for the Electronics and Telecommunications Research Institute, Daejeon, Republic of Korea as a researcher since 2022 in the Quantum Technology division. His main research interests include the development of a quantum internet and the integration of nonlinear waveguides for quantum networks.

Jiho Park received his BS, MS, and PhD degrees in physics from the Department of Physics, Pusan National University (PNU), Pusan, Republic of Korea, in 2016, 2018, and 2021, respectively. From 2021 to 2023, he worked at the Quantum

Sensor Research Center at PNU. Since 2023, he has been with the Electronics and Telecommunications Research Institute, Daejeon, Republic of Korea, where he is currently a researcher. His primary research interests are atomic physics and quantum optics.

Jaegyu Park received his BS, MS, and PhD degrees in physics from Chungnam National University (CNU), Daejeon, Republic of Korea, in 2000, 2002, and 2009, respectively. From 2009 to 2011, he worked as a postdoctoral research fellow at the Institute of Quantum Systems at CNU. He has been working at the Electronics and Telecommunications Research Institute since 2011 and has been an associate professor in the Department of Quantum Information at the University of Science and Technology since 2024. His research interests include high-speed and wafer-scale heterogeneous photonic integrated circuits based on silicon and lithium niobate for quantum information technology.

Hyeon Hwang received his BS degree in physics from the Department of Physics, Korea Advanced Institute of Science and Technology (KAIST), Daejeon, Republic of Korea, in 2019. He is currently enrolled in an integrated MS and PhD program at the Department of Physics, KAIST. His main research interests include lithium niobate integrated photonics, particularly ultrafast modulation, and efficient frequency conversion.

Woojin Noh received his BS degree in physics from the Department of Physics, Korea Advanced Institute of Science and Technology (KAIST), Daejeon, Republic of Korea, in 2019. He is currently enrolled in an integrated MS and PhD program at the Department of Physics, KAIST. His main research interests include lithium niobate integrated photonics, particularly on-chip entangled photons.

Hansuek Lee received his BS, MS, and PhD degrees in electrical engineering from Seoul National University, Republic of Korea, in 2001, 2004, and 2008, respectively. From 2008 to 2011, he was a postdoctoral research fellow at the California Institute of Technology (Caltech), USA. From 2011 to 2015, he was a senior researcher staff member and a visiting associate at Caltech. In 2015, he joined the Korea Advanced Institute of Science and Technology, Republic of Korea, and has been a professor in the Department of Physics. His research interests include nonlinear phenomena in ultrahigh-Q micro–/nano-cavities, light-matter interactions, opto-mechanics, and bio-photonic phenomena in nano-structures.

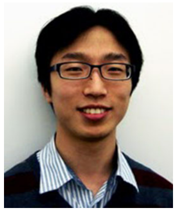

Min-Kyo Seo received his BS and PhD in physics from Korea Advanced Institute of Science and Technology (KAIST) in 2003 and 2009, respectively. In 2009, he was a research professor at Korea University, Republic of Korea. From 2009 to 2010, he was a postdoctoral research fellow at Stanford University, USA. Since 2011, he has been a professor of Physics at KAIST. His research interests lie in strong light-matter interaction in micro–/nano-resonators and its applications in optoelectronics and nonlinear/quantum optics.

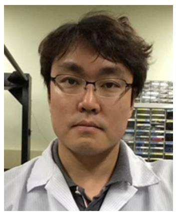

Kiwon Moon received his BS and MS degree from the electronics and electrical engineering department of Pohang University of Science and Technology (POSTECH), Republic of Korea, in 1998 and 2002, respectively, and his PhD degree in electronics and electrical engineering from POSTECH in 2011. From 2002 to 2005, he worked for Samsung Electro-Mechanics, Republic of Korea, as a senior engineer. Since 2012, he has been with the Electronics and Telecommunications Research Institute, Republic of Korea. His main research interests include quantum communication and computing.

Jung Jin Ju received his BS, MS, and PhD degrees from the Physics Department of Pusan National University, Republic of Korea, in 1990, 1992, and 1997, respectively. He worked at Korea Research Institute of Standards and Science in 1998 and Pohang University of Science and Technology in 1999. Since 2000, he has been with the Electronics and Telecommunications Research Institute, Daejeon,

Republic of Korea, where he is currently a principal researcher. His main research interests include the development of nanophotonic integrated circuit technologies for telecom, datacom, and quantum applications such as the quantum internet and quantum computing.

How to cite this article: H.-S. Kim, G. Kim, T. Slusar, J. Kim, J. Park, J. Park, H. Hwang, W. Noh, H. Lee, M.-K. Seo, K. Moon, and J. J. Ju, *Fabrication of low-loss symmetrical rib waveguides based on x-cut lithium niobate on insulator for integrated quantum photonics*, ETRI Journal **46** (2024), 783–792, DOI 10.4218/etrij.2024-0137